The turning of the wind in the atmospheric boundary layer

Alfredo Peña, Sven-Erik Gryning and Rogier Floors
DTU Wind Energy, Risø campus, Technical University of Denmark, Roskilde, DK
E-mail: aldi@dtu.dk

Abstract. Here we use accurate observations of the wind speed vector to analyze the behavior with height of the wind direction. The observations are a combination of tall meteorological mast and long-range wind lidar measurements covering the entire atmospheric boundary layer. The observations were performed at the Høvsøre site in Denmark, which is a flat farmland area with a nearly homogeneous easterly upstream sector. Therefore, within that sector, the turning of the wind is caused by a combination of atmospheric stability, Coriolis, roughness, horizontal pressure gradient and baroclinity effects. Atmospheric stability was measured using sonic anemometers placed at different heights on the mast. Horizontal pressure gradients and baroclinity are derived from outputs of a numerical weather prediction model and are used to estimate the geostrophic wind. It is found, for these specific and relatively short periods of analysis, that under both barotropic and baroclinic conditions, the model predicts the gradient and geostrophic wind well, explaining for a particular case an 'unusual' backing of the wind. The observed conditions at the surface, on the other hand, explain the differences in wind veering. The simulated winds underpredict the turning of the wind and the boundary-layer winds in general.

1. Introduction

So far we have mainly focused our efforts on investigating the influence of the vertical wind shear on wind turbines, as shown in several studies (see refs. [1–6]). However, with the installation of modern large turbines, we also need to understand their response to wind direction shears (turning of the wind) within the rotor layer and in the entire atmospheric boundary layer (ABL), as wind turbines are sometimes operating above the boundary-layer height (BLH).

The idea of this study is therefore to give a first look at the influence of features such as atmospheric stability, and horizontal pressure and temperature gradients on the results of the analysis of high quality observations of the wind speed vector, looking in particular at the turning of the wind. Some of these features can be estimated from routinely available observations of the turbulent fluxes. Others, such as the above mentioned gradients, can be easily estimated from numerical simulations, for example from mesoscale model outputs.

The observations are here carried out with a long-range wind lidar on a place in north Europe with 'nearly ideal' topographical conditions, which allow us to study the basic mechanisms controlling the behavior of the turning of the wind, given the type of atmosphere and forcing (geostrophic) conditions at the site. We use mesoscale model simulations not only to understand the large-scale conditions, but also to evaluate the ability of the model to predict the turning of the wind.

2. Background

The surface geostrophic winds are estimated as (see ref. [7]),

$$G_{o_x} = -\frac{1}{\rho\, f_c}\frac{\partial P_o}{\partial y}, \quad G_{o_y} = \frac{1}{\rho\, f_c}\frac{\partial P_o}{\partial x}, \tag{1}$$

where ρ is the air density, f_c the Coriolis parameter, and P_o the mean sea level pressure. x and y refer to two perpendicular directions. The thermal winds account for the effect of baroclinity and can be derived as ref. [8],

$$G_{Tx} = -\frac{1}{f_c}\frac{\partial\left(\Phi_z - \Phi_o\right)}{\partial y}, \quad G_{Ty} = \frac{1}{f_c}\frac{\partial\left(\Phi_z - \Phi_o\right)}{\partial x}, \tag{2}$$

where Φ is the geopotential given at a certain height z and at the surface o. The geostrophic wind at any level is found by adding the surface geostrophic and the thermal wind. The thermal wind is zero in barotropic conditions and a function of height in baroclinic conditions. In this study we use the gradient wind G_g near the surface, which is the surface geostrophic wind corrected for the effect of the curvature of the isobars (see ref. [9] for further details). The geostrophic wind at any level is found in this paper by adding the thermal wind to the gradient wind computed near the surface, i.e. assuming advection and other dynamic effects are negligible.

3. Measurements and modelling

We combine sonic anemometer measurements at 10, 40, and 100 m above ground level (all heights are here referenced to the ground) with wind lidar observations performed at the Høvsøre site in Denmark. The site and the wind lidar measurements are well documented in refs. [10–12] and the other references therein. This study focuses on easterly winds at Høvsøre, where the terrain is flat and nearly homogeneous. The wind lidar is a WLS70 pulsed WindCube measuring the 3D wind vector from 100 up to 2000 m every 50 m. We use the wind lidar's carrier-to-noise ratio (CNR) of −22 dB (based on 10-min averages) to filter data. We implement a stationarity filter (see details in ref. [12]) and the final analysis is performed over 30-min averages, i.e. we complement 30-min averages of sonic parameters with the wind lidar measurements.

The Weather Research and Forecast (WRF) model version 3.4 was used to perform simulations over an area larger than Denmark. Details about the model setup and the simulations are given in refs. [12, 13] and at `http://veaonline.risoe.dk/tallwind/tallwindcases.html`. Instantaneous outputs from the WRF simulations, corresponding to the periods of combined sonic/wind lidar observations, are extracted and also averaged in 30-min means. This includes the model simulated BLH (see details related to its computation in ref. [14]). Sea-level pressure and geopotential horizonal gradients are computed from the simulated fields over a 300 km×300 km square around the Høvsøre site. More details about the estimation of the large-scale winds from the mesoscale simulations, as well as details such as land mask, land cover, and roughness description, are given in refs. [10–12, 15].

4. Results

Five different cases of 'boundary-layer' profiles are here described (more details and cases are given in ref. [12]). The cases are ensemble means of 30-min averages of wind speed and related parameters, which are both observed and simulated. The variability of the cases can be found under the weblink mentioned above. The criteria used to categorize the observations/simulations into the five cases are basically that the 30-min averages have: 1) similar observed wind speed and turning of the wind conditions (differences less than 20%) at 100 m and 2) similar observed surface turbulent fluxes (differences less than 20% in friction velocity at 10 m) and so atmospheric stability and simulated forcing conditions.

For all cases we show 2D (horizontal plane) plots (Figs. 1–5) of the observed surface wind vector, specifically the 10-m wind $\mathbf{U_{10}}$, the observed wind vector close to the simulated BLH $\mathbf{U_{BLH}}$, and the observed wind vector at a level between the surface and the BLH. From the simulation side we show the first model level wind vector $\mathbf{U_{14}}$ and that close to the simulated BLH $\mathbf{U_{BLH}}$, the gradient wind at the first model level $\mathbf{G_{14}}$, and the geostrophic wind close to the simulated BLH $\mathbf{G_{BLH}}$.

4.1. Case 1: Very stable surface atmosphere, low forcing, and high wind veering
These conditions were observed in a morning of early May and lasted for about two hours. The observed wind veers 43° in the first 100 m (the simulated BLH is about 87 m) and continues veering high above. As seen in Fig. 1, the observed wind speeds are about the cut-in values of most common wind turbines and so these might operate under the high veer and shear observed conditions.

The simulated winds highly underestimate the veer, and the simulated BLH wind, in particular, is highly misaligned with the observation at the same level. The observed very stable surface atmosphere (with very low momentum flux) explain the difficulties for wind modeling under these conditions using WRF (see `http://veaonline.risoe.dk/tallwind/cases/case1.txt` to extract the two horizontal wind speed components, u aligned with the 10-m wind and v perpendicular to it, the two components of the simulated geostrophic wind, the friction velocity and a dimensionless stability parameter from 10–100 m, and a measure of the variability of the observations). Interestingly, the simulated gradient and the geostrophic BLH winds are in very good agreement with the observed BLH wind. Baroclinity is not causing the severe observed wind shear and veer, as these two simulated large-scale winds are nearly equal (at least at this height).

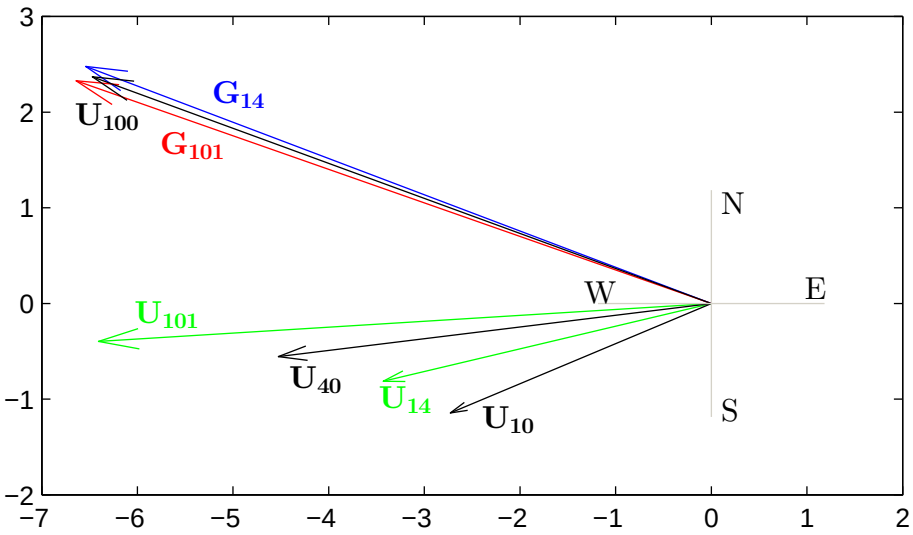

Figure 1. Horizontal wind speed vectors observed at 10 m, close to the BLH and a level in between (in black), simulated winds at the first model level 14 m and that at the BLH (in green), simulated gradient wind (in blue) and simulated geostrophic wind at the BLH (in red) for case 1. The axes show the wind speed magnitudes in m s^{-1} for both north-south and east-west directions

4.2. Case 2: Highly baroclinic atmosphere and low-level jet

These conditions were observed during four hours around midnight in late April. The observed wind veers 61° in the first 500 m (the simulated BLH is 351 m) and there is an observed wind maximum of 20.1 m s^{-1} at 400 m (not shown) due the presence of a low-level jet (LLJ). The observed stable atmosphere at the surface combined with the LLJ partly explain the high shear and veer in the observed conditions (see refs. [10, 12, 16]). The observations for the case are provided at `http://veaonline.risoe.dk/tallwind/cases/case3.txt`.

The simulated winds show an angle offset at the two comparable levels, but they just slightly underestimate the wind veer. They highly underestimate the LLJ maximum and so the wind shear (see Fig. 2). The simulated geostrophic 485-m wind $\mathbf{G_{485}}$ is rather well aligned with the observation at the closest level (although the observed wind is highly ageostrophic as expected) and the difference between the gradient wind $\mathbf{G_{14}}$ and $\mathbf{G_{485}}$ is due to the added thermal wind, which is mainly due to a positive temperature difference northwards.

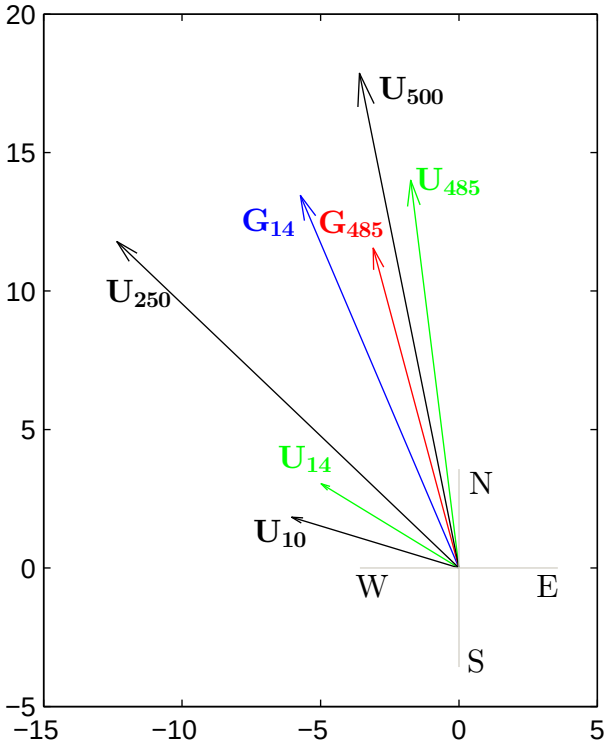

Figure 2. Same as in Fig. 1 but for case 2

4.3. Case 3: High forcing and stable surface conditions

These conditions were observed during ≈ 15 hours in the early morning and late night periods of two days in early September. The wind veers 45° in the first 700 m (the simulated BLH is 763 m) and all observed wind speeds are rather high as seen from Fig. 3. The observed surface conditions are stable, explaining the relatively high wind shear observed (see refs. [2, 4]), particularly seen in the difference between $\mathbf{U_{10}}$ and $\mathbf{U_{350}}$ (see `http://veaonline.risoe.dk/tallwind/cases/case4.txt`).

As in Case 2, the simulated winds show an angle offset at the comparable levels and a slight underestimation of the wind veer. The BLH wind is fairly well estimated by the simulations. The high simulated large-scale winds explain the high wind speeds observed and, most interestingly,

both simulated gradient and geostrophic BLH winds are perfect estimators of the observed BLH wind, indicating, among others, that the atmosphere is very close to barotropic.

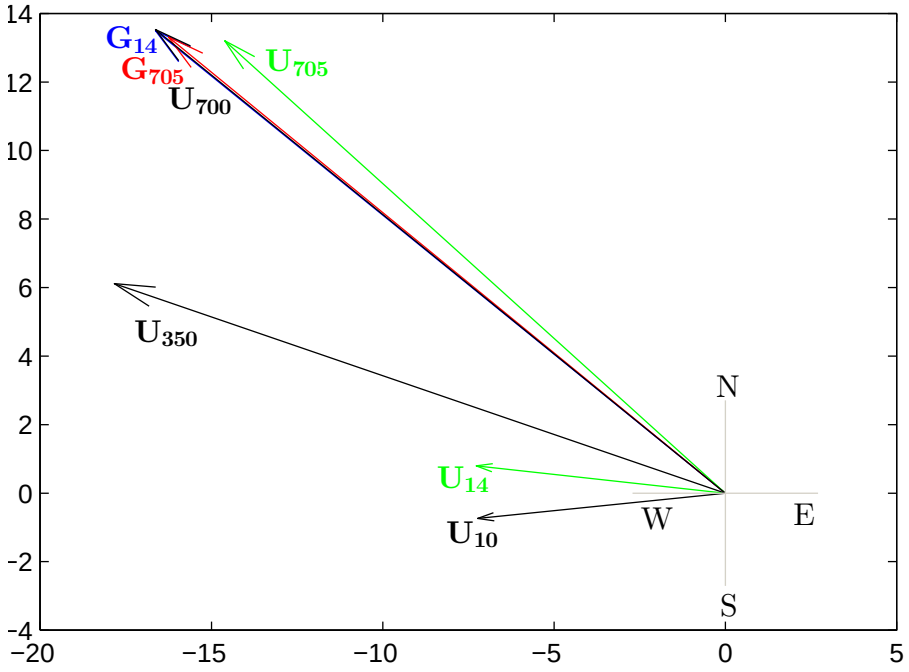

Figure 3. Same as in Fig. 1 but for case 3

4.4. Case 4: Barotropic atmosphere and neutral surface conditions
These conditions were observed during the early afternoon hours of three days in early September. The observed wind veers 25° within the first 1200 m (the simulated BLH is 1120 m and matches the height of the observed wind maximum). The observed conditions at the surface are neutral (with high momentum flux measured by the sonics), which combined with the high simulated large-scale winds explain the high wind observed at all levels as illustrated in Fig.4 (see `http://veaonline.risoe.dk/tallwind/cases/case5.txt`).

The simulated BLH wind compares very well with the observed BLH wind (in terms of magnitude and alignment) and so the difficulties of the model to reproduce the observed wind veer are clearly illustrated. The simulated gradient and geostrophic BLH winds are very close to each other (slightly misaligned with the observed BLH wind), resulting in a nearly barotropic atmosphere.

4.5. Case 5: Highly baroclinic atmosphere and stable surface conditions
For this last case, the conditions were observed for about 2 hours in the morning of a day in the middle of December. The observed wind only veers in the first 100 m and backs 8° within the first 1000 m (the simulated BLH is 971 m; see Fig. 5). The observed surface conditions are stable with a low and constant friction velocity (see `http://veaonline.risoe.dk/tallwind/cases/case10.txt`).

The simulated winds do not show backing but a slight veering, a misalignment with the surface wind, and an underestimation of the BLH wind when compared to the observations. Most interesting is that the simulated gradient and geostrophic BLH winds are far from each other; the latter predicts well the observed BLH wind explaining the observed backing as a result of a high baroclinic component (about 6 m s^{-1} at 966 m), which points southwards. Such a

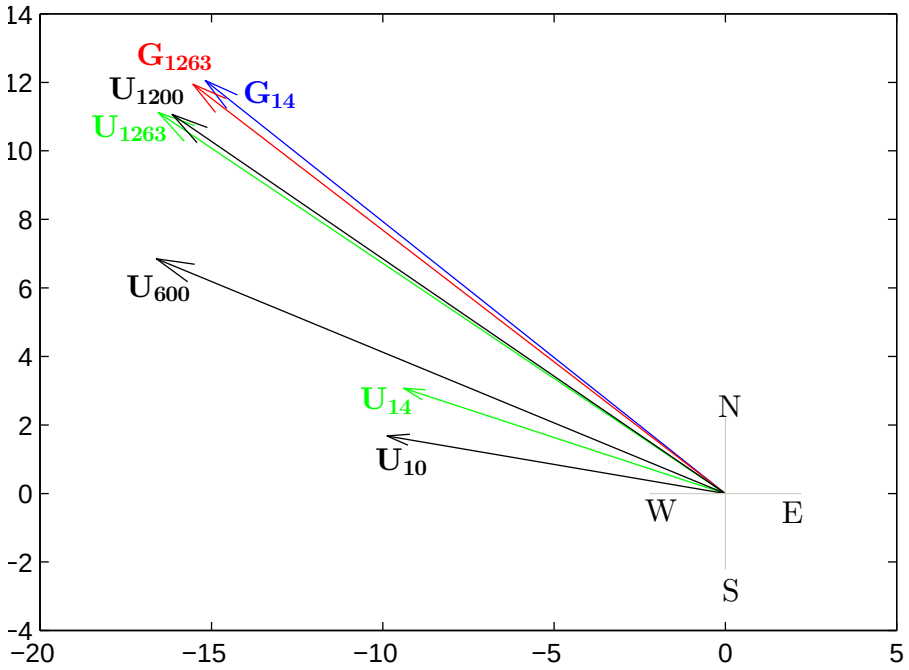

Figure 4. Same as in Fig. 1 but for case 4

thermal wind component is due to a large positive air temperature gradient eastwards (the land is colder than the sea at Høvsøre in the winter period).

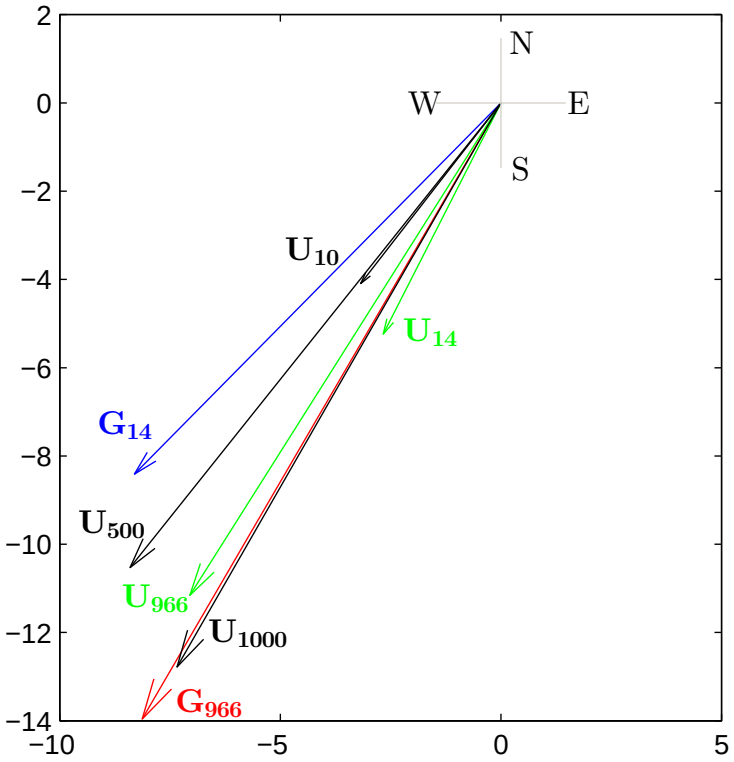

Figure 5. Same as in Fig. 1 but for case 5

5. Conclusions and discussion

The main points resulting from this analysis are:

- Under barotropic conditions (as seen from the analysis of WRF simulations of the gradient and geostrophic winds), the wind veers about 25° and 45° in neutral and stable conditions, respectively, within the entire ABL.
- Under baroclinic conditions (also from the point of view of the simulations), the observed wind can be much higher than the simulated gradient wind, in order to approach the simulated geostrophic wind. When the horizontal temperature gradient is large enough and opposite to the direction of the surface wind, the observed wind can back (i.e. the wind turns anticlockwise in the northern hemisphere).
- WRF simulated winds underestimate the observed turning of the wind within the ABL, although they reproduce the strength of the wind well, with a general and slight underprediction of the wind speed particularly close to the BLH. The simulated surface wind shows a systematic misalignment compared to the observed surface wind.
- Although the WRF simulated winds might be misaligned with respect to the observations, the simulated geostrophic and gradient winds seem to reproduce well the large-scale features at Høvsøre and compare well with the observed BLH winds.
- During an LLJ episode the model performs poorly in terms of wind, and it is illustrated that the observed BLH wind is highly ageostrophic, as expected.

Some of these points have already been explored and studied by the atmospheric modeling community. In particular, WRF has been found to poorly represent turbulent parameters such as momentum and heat fluxes, and thus atmospheric stability (see refs. [17–19]). High sensitivity to predict fluxes is generally attributed to the choice of PBL scheme; the model setup (e.g. the model horizontal resolution) does not show that high sensitivity. Friction velocity is normally found to be overpredicted by all WRF PBL schemes, which leads to an 'underprediction' of the stability; for the stable cases in particular, this generally results in a model underprediction of both wind shear and veer.

For the accurate prediction of LLJs, the model should predict intermittent turbulence well, but it has been found that the model is generally too "diffusive", producing a strong mixing especially in the first 100–300 m. This results in fewer LLJs cases compared to observations, in inversion heights at higher levels in the atmosphere than those observed, and thus LLJ (and general wind) strength underprediction.

Acknowledgements

We acknowledge funding from the Danish Council for Strategic Research Project Number 2104-08-0025 for the support of the "Tall Wind" project.

References

[1] Holtslag A A M 1984 *Bound.-Layer Meteorol.* **29** 225–250
[2] Gryning S E, Batchvarova E, Brümmer B, Jørgensen H and Larsen S 2007 *Bound.-Layer Meteorol.* **124** 251–268
[3] Peña A 2009 Sensing the wind profile Tech. Rep. Risø-PhD-45(EN) Risø DTU
[4] Peña A, Gryning S E and Hasager C B 2010 *Theor. Appl. Climatol.* **100** 325–335
[5] Muñoz-Esparza D, Cañadillas B, Neumann T and van Beeck J 2012 *J. Renew. Sustain. Energy* **4** 063136
[6] Draxl C, Hahmann A N, Peña A and Giebel G 2014 *Wind Energy* **17** 39–55
[7] Stull R B 1988 *An introduction to boundary layer Meteorology* (Kluwer Academic Publishers)
[8] Holton J R and Hakim G J 2004 *An introduction to dynamic meteorology* (Elsevier Academic Press, fourth edition)
[9] Kristensen L and Jensen G 1999 Geostrophic winds in Denmark: a preliminary study Tech. Rep. Risoe-R-1145(EN) Risø National Laboratory Roskilde, Denmark

[10] Floors R, Vincent C L, Gryning S E, Peña A and Batchvarova E 2013 *Bound.-Layer Meteorol.* **147** 469–491
[11] Peña A, Gryning S E and Hahmann A N 2013 *J. Geophys. Res. Atmos.* **118** 1924–1940
[12] Peña A, Floors R and Gryning S E 2014 *Boundary-Layer Meteorol.* **150** 69–89
[13] Gryning S E, Batchvarova E, Floors R, Peña A, Brümmer B, Hahmann A N and Mikkelsen T 2014 *Boundary-Layer Meteorol.* **150** 167–184
[14] Hong S Y, Noh Y and Dudhia J 2006 *Mon. Wea. Rev.* **134** 2318–2341
[15] Floors R, Peña A and Gryning S E 2014 *Q. J. Roy. Meteorol. Soc.* In press
[16] Peña A, Gryning S E and Mann J 2010 *Q. J. Roy. Meteorol. Soc.* **136** 2119–2131
[17] J A Gibbs E F and van Eijk A M J 2011 *J. of Applied Meteorol.* **50** 2429–2444
[18] Shin H H and Hong S Y 2011 *Bound.-Layer Meteorol.* **139** 261–281
[19] Steeneveld G J, Tolk L F, Moene A F, Hartogensis O K, Peters W and Holtslag A A M 2011 *J. Geophys. Res.* 116:D23114